Mon. Not. R. Astron. Soc. **000**, 1–8 (2016) Printed 14 July 2016 (MN LATEX style file v2.2)

Using the 2-MASS Photometric Redshift Survey to optimise LIGO Follow-Up Observations

Elisa Antolini[1], Jeremy S. Heyl[⋆2]
[1] *Dipartimento di Fisica e Geologia, Università degli Studi di Perugia, I-06123 Perugia, Italia*
[2] *Department of Physics and Astronomy, University of British Columbia, 6224 Agricultural Road, Vancouver, BC V6T 1Z1, Canada*

Accepted 2016 July 13. Received 2016 July 12; in original form 2016 February 24

ABSTRACT
The initial discovery of LIGO on 14 September 2015 was the inspiral merger and ringdown of the black hole binary at a distance of about 500 Mpc or a redshift of about 0.1. The search for electromagnetic counterparts for the inspiral of binary black holes is impeded by coarse initial source localisations and a lack of a compelling model for the counterpart; therefore, rapid electromagnetic follow-up is required to understand the astrophysical context of these sources. Because astrophysical sources of gravitational radiation are likely to reside in galaxies, it would make sense to search first in regions where the LIGO-Virgo probability is large and where the density of galaxies is large as well. Under the assumption that the probability of a gravitational-wave event from a given region of space is proportional to the density of galaxies within the probed volume, one can calculate an improved localisation of the position of the source simply by multiplying the LIGO-Virgo skymap by the density of galaxies in the range of redshifts. We propose using the 2-MASS Photometric Redshift Galaxy Catalogue for this purpose and demonstrate that using it can dramatically reduce the search region for electromagnetic counterparts.

Key words: gravitational waves: Physical Data and Processes – galaxies: distances and redshifts: Galaxies – methods: observational: Astronomical instrumentation, methods, and techniques

1 INTRODUCTION

LIGO has recently begun to detect gravitational wave events from the local Universe (Abbott et al. 2016). During these initial years of gravitational astronomy, the localisation of the candidate events on the sky is coarse with the ninety-percent confidence regions covering hundreds or even thousands of square degrees . (Kasliwal & Nissanke 2014; Singer et al. 2014; Berry et al. 2015; Abbott et al. 2016). Finding an electromagnetic counterpart to these candidate gravitational-wave events will be crucial to understand the host environment, the evolution of the progenitor and to provide tests of cosmology by yielding measurement of the redshift of the source. The ideas of how the the electromagnetic counterparts would appear are varied and uncertain. There has been substantial consideration of the electromagnetic transients associated with the mergers of binaries that include a neutron star (e.g. East et al. 2016; Kawaguchi et al. 2016; D'Orazio et al. 2016; Fernández & Metzger 2015; Mingarelli et al. 2015; Kyutoku et al. 2015; Siegel & Ciolfi 2015b,a) However,the first discovered gravitational wave event (GW150914) was almost certainly the merger of binary black holes, so the appearance and duration of the electromagnetic counterparts are especially uncertain with only a few models (e.g. Gerosa et al. 2015; Margalit & Piran 2015; Cerioli et al. 2016; Yang & Zhang 2016). Consequently, rapid electromagnetic follow-up of a large portion of the probable region would increase the chance of success in finding a counterpart. Over the large search regions and over the span of days or weeks, many electromagnetic transients typically occur, and with the wide variety of models it will be difficult to associate unambiguously a particular electromagnetic event with a candidate gravitational-wave event.

The purpose of this paper is to present a strategy to alleviate both of these issues; that is, to reduce both the search region and the time required to plan and begin observations. We follow the approach of Gehrels et al. (2015) to develop a galaxy catalogue to guide the observational plan (see also Nuttall & Sutton 2010; Hanna et al. 2014; Ghosh & Nelemans 2015; Fan et al. 2015; Bartos et al. 2015). However, our goal here is to develop a nearly complete catalogue at the

⋆ Email: heyl@phas.ubc.ca; Canada Research Chair

expense of having less accurate estimates of the redshifts of the galaxies within the catalogue. The accuracy of the galaxy distances needs to be only as good as the distance estimates of the gravitational-wave events. Additionally we will outline a straightforward and rapid technique to generate a nearly optimal observing plan to follow up the events rapidly (i.e. within a few seconds of the trigger).

2 BAYESIAN APPROACH TO FOLLOW-UP

Because we will be interested in the rapid follow-up of candidate gravitational-wave events, we will be focused on the rapid Bayesian reconstruction outlined by Singer & Price (2016), BAYESTAR. BAYESTAR yields a probability map on the sky in the form of a HEALPix map (Górski et al. 2005) where each pixel contains the posterior probability $P(m|d)$ of a particular model parameterised by the position on the sky conditioned on the observed data (i.e. the observed strains on the LIGO and Virgo interferometers). To plan an observing strategy one would like the probability of a particular model (i.e. position on the sky). We have from Bayes's theorem

$$P(\text{position}|\text{data}) = \frac{P(\text{position})P(\text{data}|\text{position})}{P(\text{data})}. \quad (1)$$

If we make the additional mild assumption that gravitational-waves originate from nearby galaxies, the probability of a given position on the sky naturally is proportional to the density (or perhaps the luminosity density) of galaxies in that direction integrated over distance range determined from the modelling of the gravitational waveform. Of course, these distance estimates will usually have large uncertainties so the distance range over which to integrate the galaxy density distribution will also be large, so highly accurate redshift information is not needed to construct $P(\text{position})$.

Furthermore, because we will ultimately be interested in which fields to observe (not which particular galaxies), accurate positions are not required in the construction of $P(\text{position})$. Because the LIGO probability maps are sampled on a HEALPix grid, it is convenient to sample $P(\text{position})$ also as a HEALPix grid with each pixel covering about the same solid angle as the field of view of the telescope of interest or the BAYESTAR map. We choose a HEALPix map with `NSIDE` $= 512$ or about 50 square arcminutes per pixel, so positions no more accurate than arcminutes are required. The key to generate the observing plan rapidly is to calculate the required galaxy density maps beforehand in principle at the desired resolution (this optimisation only speeds the process up slightly) for the distance ranges of interest. With the arrival of an alert, all that is required is to calculate Eq. (1) using the HEALPix maps, resample to the scale of the telescope, renormalise the probability, sort the pixels from most likely to least and output the positions to cover a given amount of cumulative probability (this entire process takes typically less than one second).

3 GALAXY CATALOGUES

To gain a picture of the local Universe, our focus will be the completeness of the data rather than the accuracy of the distances and positions. The Census of the Local Universe (CLU; Gehrels et al. 2015) combines several redshift surveys (2dF Galaxy Redshift Survey Norberg et al. 2002; the Millenium Galaxy Catalog, Liske et al. 2003; Driver et al. 2005; and the 2MASS Reshift Survey Huchra et al. 2012) that cover a large portion of the sky, but at various depths and attempt to increasing the completeness of the sample by using only the galaxies near the upper-end of the luminosity function (*i.e.* $L \sim L_*$). This may optimise the strategy to discover neutron-star binaries whose abundance is probably proportional to the total number of stars in a galaxy, and galaxies near L_* dominate the stellar mass in the Universe (however see Leibler & Berger 2010, for caveats to this assumption). On the other hand, the discovery that binary black holes with large masses dominate the initial detections indicates that focusing the search on massive galaxies might not be the best strategy to discover the electromagnetic counterparts to the first sources. After all such large black holes have not been found so far in our approximately L_*-galaxy, the Milky Way, or our neighbour, Andromeda. In fact theoretical arguments indicate that the production of such massive black holes results from the evolution of massive stars in low metallicity galaxies (Abbott et al. 2016a; Eldridge & Stanway 2016) which are typically small in the local Universe (e.g. Heyl et al. 1997). Our goal is to have a nearly complete survey that attempts to be unbiased with respect to the mass of the galaxy.

We follow in spirit the work of Jarrett (2004) who used The Two Micron All Sky Survey extended source catalogue (2MASS XSC, Jarrett et al. 2000b; Skrutskie et al. 2006), and the assumption that all galaxies have the same K_s-band luminosity of around L_* to estimate distances to each galaxy and create sky maps of the local Universe. A substantial fraction of 2MASS has measured redshifts (e.g Huchra et al. 2012). Bilicki et al. (2014) combined the photometric data from 2MASS XSC with additional photometry the mid-infrared from WISE (Wright et al. 2010) and the optical from SuperCOSMOS (Hambly et al. 2001a,b,c). Using this multiband photometry, they trained neural networks using measured spectroscopic redshifts from SDSS (Ahn et al. 2012, 2014), 2dF (Colless et al. 2001, 2003), 6dF (Jones et al. 2004, 2009) and other catalogues to determine photometric redshifts. They also extend the photometric redshift catalogue beyond the 2MASS XSC building a three-dimensional map of the sky out to a redshift of nearly 0.2 well into the realm of the first gravitational wave event. The 2MASS Photometric Redshift (2MPZ) catalogue contains over one million galaxies with a median redshift of 0.1 with a typical scatter between the photometric and spectroscopic redshifts (where both are known) of $\sigma_z = 0.015$.

Except for the most local binary-black-hole mergers and neutron-star-black-hole mergers, the estimated distances from the gravitational wave data itself have comparable errors to this, so this catalogue is sufficiently accurate to calculate the surface density of galaxies with the expected redshift range of a particular gravitational-wave detection. On the other hand, the binary-neutron-star sources will have distances comparable to these uncertainties. Fortunately, for these nearby sources, there are nearly uniform all-sky redshift surveys which would be more appropriate for this task (e.g. Saunders et al. 2000; Huchra et al. 2012). Of course, all of the techniques outlined here can be applied to these more

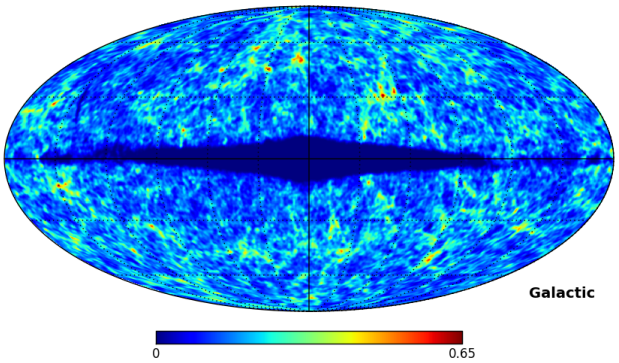

Figure 1. The relative surface density of galaxies in the 2-MASS Photometric Redshift Survey with photometric redshifts between 0.01 and 0.1, smoothed with a Gaussian of 0.6 degrees (0.01 radian).

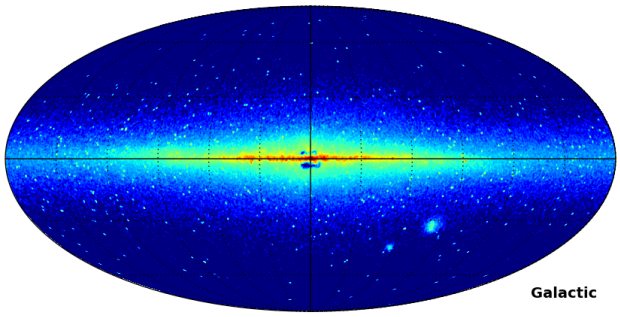

Figure 2. The relative surface brightness of stars in the 2-MASS Photometric Catalogue (Skrutskie et al. 2006) smoothed with a Gaussian of 0.03 degrees (0.005 radian).

nearby catalogues to produce sky maps of even more nearby galaxies. Here we will focus on galaxies with photometric redshifts between 0.01 and 0.1 from the 2MPZ catalogue as depicted in Fig. 1. For closer galaxies the redshift error is significant (the mean error is about 0.015), and the outer end of the range is both the median redshift of the catalogue and the typical distances of the binary-black-hole sources. Although at the inner edge of the catalogue the redshift error exceeds the redshift estimate, this does not impede our goal of creating a catalogue of nearby galaxies to look for counterparts to binary-black-hole mergers.

To produce this map we divided the sky into 3,145,728 regions (each of about 45 square arcminutes, four ACS fields) using a HEALPix (Górski et al. 2005) tessellation with `NSIDE` = 512. Each cell of the map simply contains the number of galaxies in the 2MPZ catalogue within the range of photometric redshift that lie within that portion of sky. We have consequently smoothed the map with a Gaussian of 0.6 degrees or about 2 Mpc at a redshift of 0.05. This smoothing accounts for the possibility that either the binary-black hole has been kicked out of one of the catalogue galaxies (1000 km/s for 1 Gyr yields 1 Mpc) or that the catalogue galaxies are accommpanied by smaller galaxies that are absent from the catalogue but cluster around those in the catalogue within a typical group scale of 1 Mpc. In prinicple we could smooth the maps more finely with increasing distance; these results would necessarily be closer to the unsmoothed map.

Typically no HEALPix pixel contains more than one galaxy from the catalogue. After smoothing we notice the large-scale structure even when we have averaged over distance. This demonstrates the potential optimisation in the observing strategy by observing fields with nearby galaxies. Depending on whether one believes that the sources are associated with the visible portion of galaxies or may travel some distance from the galaxy itself before the gravitational-wave event, one would use either the raw galaxy counts or the smoothed map.

Furthermore, our choice of weighting the fields simply by the number of galaxies within each field is perhaps the most simple one. Given the type of event, one could use a map that gives small, low-metallicity galaxies more weight or weigh the galaxies by their mass or luminosity. Of course, all of these possibilities would be informed by one's prior knowledge of the source guided by theoretical models and the hints from the waveform itself and give a better estimate of P(position). The key is to calculate these maps beforehand.

There is a further structure apparent in the map, and this is the zone of avoidance imposed by the disk and bulge of our Galaxy. Depending on the nature of the follow-up (*e.g.* gamma-ray and radio) observations it may make sense to include regions along the Galactic plane where one thinks nearby galaxies should be. One can attempt to probe the zone of avoidance (e.g Jarrett et al. 2000a) and future 21-cm surveys like CHIME (Vanderlinde & Chime Collaboration 2014) will also probe the large-scale structure beyond the Galactic plane. However, the existing galaxy density map as depicted in Fig. 1 can yield an estimate of the structure obscured by the Galaxy. The technique that we will use in similar to that used by Abrial et al. (2008) to inpaint the CMB anisotropies across the Galactic plane.

Here we will determine the region masked by the Galaxy by finding the region in which the density of galaxies is either less than one tenth of the mean (from Fig. 1) or in which the density of stars (from Fig. 2) is greater than a threshold that accounts for the masking of the background galaxies due to the Large Magellanic Cloud, a feature that is apparent in both figures. Both of these masks are nearly the same, so we combine them as depicted in the upper panel of Fig. 4. This region is much narrower than the infilled region of the CMB in Abrial et al. (2008), and furthermore the observed structures the galaxy map are typically longer than the width of the mask, so we can reliably estimate the hidden structures. In spite of these differences the basic strategy is similar. We assume that the underlying galaxy map (behind the Galaxy) is isotropic; therefore, it is natural to represent it as a sum of spherical harmonics; furthermore, we can argue that a small fraction of the components contain most of the power, *i.e.* the representation of the underlying map is sparse, so we can use the adaptive thresholding strategy of Bobin et al. (2007) to estimate the underlying galaxy distribution. Caiazzo et al. (2016) give the details of the procedure as well as a variety of tests.

To demonstrate its efficacy here, we will first apply the procedure to a galaxy map that has an additional mask as depicted in Fig. 3. We have masked both the Galactic plane

and the equatorial plane. These equatorial region outside the Galactic plane is our test region where we know the underlying galaxy distribution, and we attempt to reconstruct it from the data outside the masked regions. Most of the structures within the equatorial region in the top panel are reproduced in the lower middle panel. The difference between the input map and the infill map is depicted in the bottom panel. To make statistic sense of the agreement we calculate Pearson's correlation coefficient (r) between the original data and the infilled reproduction within the infilled region outside of the Galactic plane. We obtain a value of $r = 0.25$. To estimate the significance of this value, we perform two tests. First, we shuffled the data within the test region and recalculated r for these shuffled sets. Over one thousand trials the maximum value of r obtained was 0.0057 and the distribution was consistent with a normal distribution with $\sigma = 0.002$ and a mean of zero or approximately the reciprocal of the square root of the number of pixels within the test region. For an second more stringent test we calculated the angular power spectrum of the original galaxy map and generated 1,000 galaxy maps consistent with this power spectrum. This accounts for the fact that neighbouring regions of sky are correlated, which the standard shuffle test neglects. The largest obtained was 0.171, and the distribution was consistent with a normal distribution with $\sigma = 0.066$ and zero mean, so the observed correlation over the test region reaches nearly four-sigma significance. For comparision the correlation coefficient of the galaxy map with a bootstrapped realisation of the same map over the test region is typically much higher $r = 0.97$, so clearly much information is lost in the reconstruction, but the test reveals that the infilling procedure does give a good first-order guess at the hidden structures.

The region that we have infilled is still apparent in the infilled map, whereas for the infilled CMB, the infilled region typically is not apparent. We believe that this results from two facts. First, we are infilling a narrow region, so that we can get as reliable an estimate of the background galaxy distribution as possible. For the CMB infilling one just wants a map that is constrained to be the same outside the infilled region and has the same statistics as the rest of the map within the region; one does not need a reliable estimate of the covered sky, so one can mask a larger portion of the image. The second reason is that the galaxy density is strictly positive whereas at the CMB anisotropies are positive and negative. We have tried some simple reparametrisations of the galaxy density, but these either yield the same artifacts (such as subtracting the mean desnity) or other difficulties (such as using the logarithm of the density).

After demonstrating the efficacy of the infilling procedure, we now perform the calculation to infill only through the Galactic plane (we did infill the Galactic plane in the tests as well). The upper panel of Fig 4 depicts the mask that we will use to mask the data in Fig. 1, and the middle panel gives the initial galaxy map with the masked region filled in. There are several structures within masked region that connect with the structures on either side of the Galactic plane. Finally, we can estimate the signal-to-noise of the infilled map by calculate a series of galaxy density maps by resampling the 2MPZ to obtain new catalogues, new maps and new infilled maps. The lower panel of Fig. 4 depicts the signal-to-noise ratio of the map. Outside of the Galactic plane the signal-to-noise almost everywhere exceeds four. In the infilled region most of the overdense structures correspond to high signal-to-noise regions and therefore may provide a reliable estimate of the regions in the zone of avoidance where P(Position) is large.

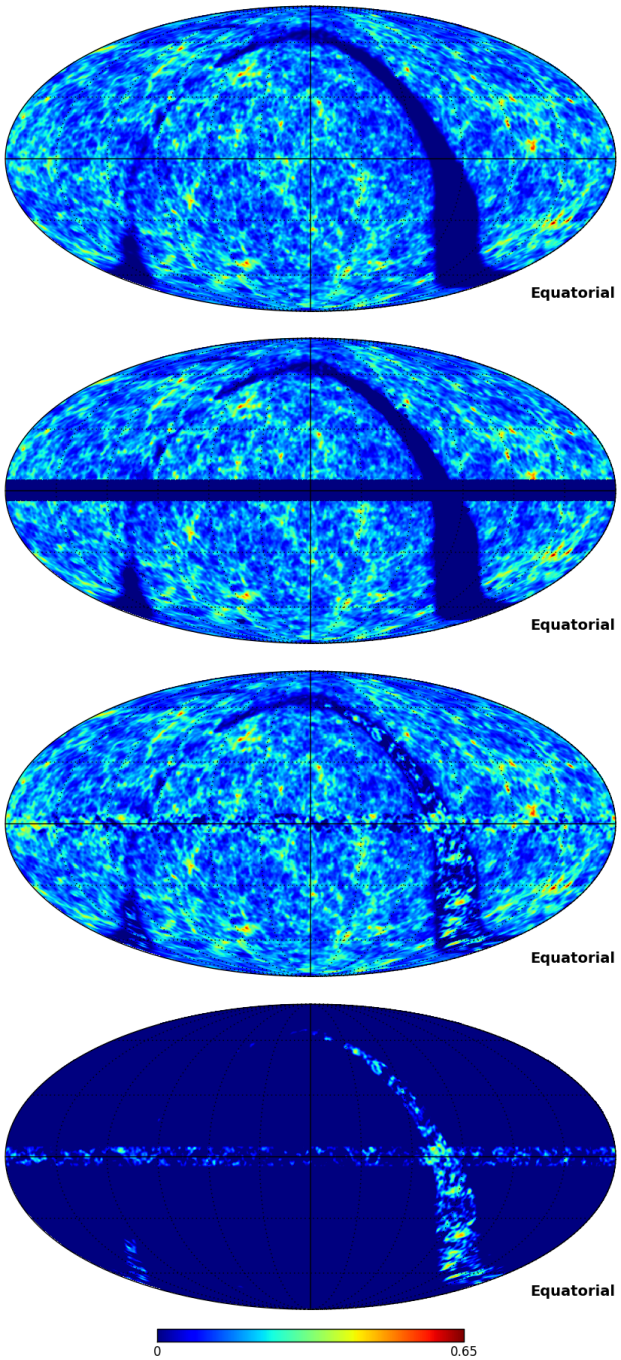

Figure 3. Top: the data used for the infilling test before masking (this is the same as Fig. 1 but in equatorial coordinated. Upper middle: we masked both the Galactic plane and within five degrees of the celestial equator. Lower middle: the infilled galaxy distribution both in the Galactic plane and the equatorial plane to compare with the upper panel. Bottom: the difference between the initial map (top) and the infilled map (lower middle).

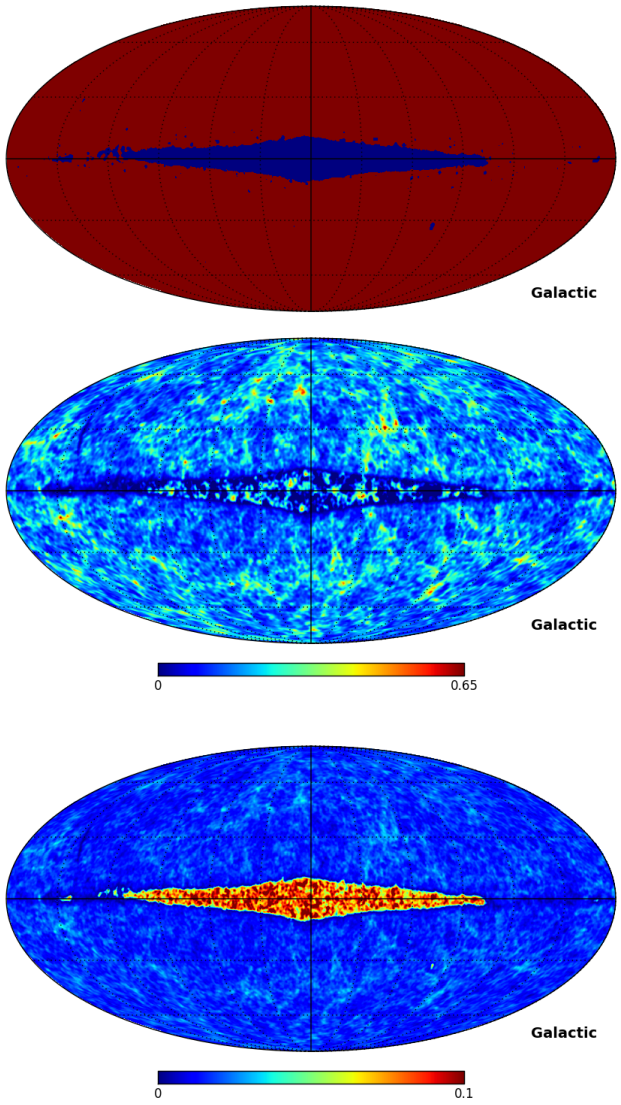

Figure 4. Upper: the mask used for the infilling procedure obtained by determining the regions where the galaxy density is less than one tenth of the mean or the star density lies above a given threshold (see text for details). Middle: the infilled galaxy distribution. Lower: The standard deviation of the infilled map obtained by bootstrapping the galaxy catalogue.

4 RESULTS

To assess the performance of these techniques we will first focus on optical follow-up where we do not wish to observe through the zone of avoidance. We will use the Bayesian probability region calculated by the BAYESTAR algorithm (Singer & Price 2016) from Singer et al. (2014) for a LIGO-only detection, that is, before Virgo is operational. For simplicity we focus on fields of view that correspond to a particular valid value of `NSIDE` for the HEALPix map. In particular we examine a 13-square-degree field of view (`NSIDE` = 16) similar to that of LSST, 0.8 (`NSIDE` = 64) and 0.05-square-degree fields of view. We quantify the performance in two ways: the time to create the optimised observing plan is typically 1-3 seconds and the decrease in the number of fields required to reach a given cumulative probability.

Fig. 5 depicts the results for the different sizes of fields and the possibility of using an raw (unsmoothed) and smoothed galaxy map. The upper panel gives the performance with a galaxy map restricted to the redshift range $0.03 < z < 0.04$. Here the improvement in the number of fields to observe is most dramatic. We begin with the lowest triplet of curves that correspond to the largest field of view. Here the improvement is of using a galaxy map is modest, the number of fields to achieve a given cumulative probability decreases by about 20%. This is because most 13-square-degree regions of the sky contain a nearby galaxy. Furthermore, with such a large field of view using a smoothed galaxy map does not affect the results significantly. On the other hand, if one uses the alternative metric of what is the probability of that the source lies within the first field, the use of a galaxy map increases this probability from about 6.6% to 14.5%.

If we now examine the most modest field of view, the 0.05 square-degree field, we can see a more dramatic advantage of using the galaxy map. If one uses the raw galaxy map in which each observed field must contain at least one galaxy, it requires 73 fields (or about 4 square degrees) to reach half of the cumulative probability. To reach the same cumulative probability requires 742 fields (about 38 square degrees) if one uses the smoothed map and 1,211 fields (about 61 square degrees) without a galaxy map. For such a small field of view the effectiveness of the galaxy map is dramatic. Furthermore, the chance of the source being in the first observed field increases from 0.07% to 1.2% with the unsmoothed map. Understandably for the intermediate-sized fields of view the improvement is intermediate between that achieved for the LSST field of view and for the modest one.

If the redshift estimate for the source is much less accurate perhaps $0.01 < z < 0.1$, the gains to be had by using a galaxy map are more modest as depicted in the lower panel of Fig. 5. The galaxy map corresponding to this range of redshift is given in Fig. 1. For the 13 square-degree field of view, the improvement is especially modest; with the galaxy map eight fields are required to reach the fifty percent mark and without the map nine fields are required. For the smallest field of view, the galaxy map reduces the number of fields required to reach the fifty-percent mark from 1,211 to 473, a 61% reduction. With the more accurate redshift estimate the reduction was nearly 94%. The probability of the source lying in the first field increases from 0.07% to 0.46%. This stresses the importance of having distance estimates as early as possible in the data analysis following a burst.

Fig. 6 depicts the results using the infilled galaxy map. An infilled map is useful to search for electromagnetic counterparts that may be seen through the Galactic plane, for example, gamma-rays, hard x-rays and radio emission. Here we use a narrower range of fields of view: 0.2, 0.8 and 3 square-degrees. For example the Parkes Multibeam receiever (Staveley-Smith et al. 1996) can cover about 3 square-degrees in a single pointing and the XMM-Netwon EPIC instrument has a 0.25 square-degree field. Here we will focus on the middle set of green curves that are for the 0.8-square-degree field of view, the same as the green curves in lower panel of Fig. 5. In both figures the upper solid curve

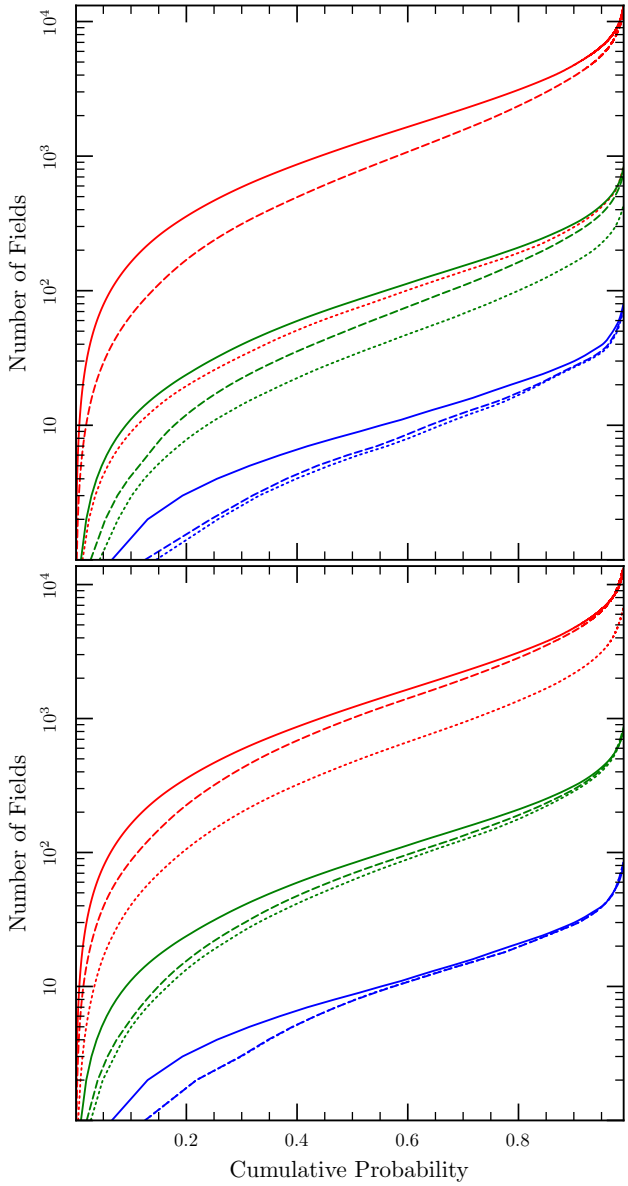

Figure 5. The number of fields required to cover the given fraction of the probability region for a simulated LIGO detection (solid curves curves without the galaxy map, dashed curves with a smoothed galaxy, dotted with a raw galaxy map). The upper red curves use a HEALPix map with about 800,000 cells, the green curves have about 50,000 cells, the blue curves have about 3,000 cells, corresponding 0.05, 0.8 and 13 square-degree fields of view. The redshift range of the galaxy map in the upper panel is $0.03 < z < 0.04$ and $0.01 < z < 0.1$ in the lower panel.

gives the number of fields without a galaxy maps and the dashed curve gives the number of fields with a smoothed galaxy map. For these curves, the first field has one-percent probabilty without a galaxy map and two percent with the smoothed galaxy map. The infilled map because it also has probablity through the Galactic plane yields an intermediate result of 1.6% in the first field. To reach half of the probability requires 84 fields without a galaxy map, 79 with the infilled map and 70 with the smoothed map, so again using the infilled map and searching through the Galactic

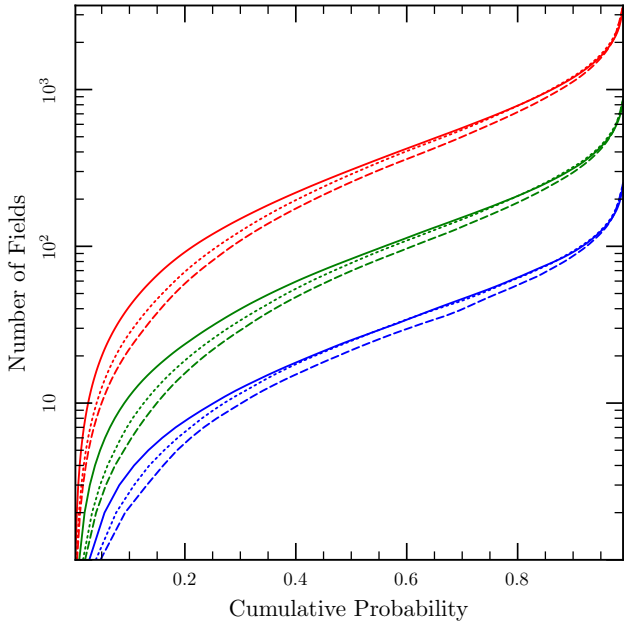

Figure 6. The number of fields required to cover the given fraction of the probability region for a simulated LIGO detection: solid curves curves without the galaxy map, dashed curves with a smoothed galaxy map and the dotted curves with a smoothed maps infilled through the Galactic plane. The upper red curves use a HEALPix map with about 200,000 cells, the green curves have about 50,000 cells, the blue curves have about 12,000 cells, corresponding 0.2, 0.8 and 3 square-degree fields of view. The redshift range of the galaxy map is 0.01 to 0.1. The green dashed and solid curves are the same as those in the lower panel of Fig. 5.

plane yields an intermediate result. One could reduce the number of fields to reach the fiftieth percentile slightly by using the infilled, smoothed map in the Galactic plane and the raw galaxy counts outside of the plane. The total number of fields required to search half of the probability is 63 for the raw map, so the improvement achieved through this additional complication is modest.

5 CONCLUSIONS

The discovery of gravitational waves from binary-black-hole mergers highlights the need for rapid three-dimensional localisation of gravitational-wave events to understand the astrophysical nature of these sources (Nissanke et al. 2013; Singer et al. 2016a,b) Although the Fermi GBM did see hints of gamma rays coincident with the gravitational wave event in time (Connaughton et al. 2016), other efforts at finding an electromagnetic counterpart only provided upper limits (e.g Abbott et al. 2016b; Soares-Santos et al. 2016; Smartt et al. 2016; Fermi-LAT collaboration 2016), possibly due to the rapid decay of the electromagnetic radiation from the binary black-hole merger. Only the GBM experiment though had observations coincident in time with the event. The Fermi LAT managed to observe the entire probability region within 70 minutes of the event, so the timescale for rapid follow-up of these events is minutes rather than hours. The algorithms presented in this paper offer a technique to maximise the potential for discovery with a very modest

computation of the fields to observe first and which order. The key is to calculate the likely regions of sky to observed before the burst in the form of a HEALPix map, so at the burst one can rapidly construct the observing plan.

The information that one puts into the map, of course, will depend on the nature of the gravitational-wave event (*e.g.* its distances, the masses and composition of the components, *etc.*). Here we have simply used the surface density of nearby galaxies for the P(position) map. However, one can do much better by using the predicted rates of the various types of events and the types of galaxies that one expects to find them in. For example, Belczynski et al. (2016) argue that an event like GW150914 resulted from a binary black hole whose progenitor stars formed around a redshift of 3 (70% likely) or around a redshift of 0.2 (30%). This information informed by stellar population synthesis could be used to develop a better guess for the galaxy map by increase the weight of galaxies whose stars were born during these epochs. Dominik et al. (2015) argue that the coalescence of black-hole binaries like GW150914 will dominate the detection rates, and furthermore, most of these binaries form in low-metallicity galaxies at about 1 Gyr after the Big Bang. Knowing in which local galaxies these systems typically end up would greatly improve the follow-up strategy. Are we interested in looking at systems that are still low metallicity with star formation long ago like dwarf spheroidals? Or do we expect these systems to have been incorporated in larger galaxies subsequently and are these larger galaxies typically spirals or ellipticals today?

The dawn of gravitational wave astronomy is upon us. To realise its full potential we can use all of our prior knowledge of the expected rates of these event in the context of the hierarchical formation of galaxies to determine where to look for the electromagnetic signal that hopefully accompanies these events.

The software and galaxy maps used in this paper is available at `http://ubc-astrophysics.github.io`. We used the VizieR Service, the NASA ADS service, the SuperCOSMOS Science Archive, the NASA/IPAC Infrared Science Archive, the HEALPy libraries and arXiv.org. This work was supported by the Natural Sciences and Engineering Research Council of Canada, the Canadian Foundation for Innovation, the British Columbia Knowledge Development Fund and the Bertha and Louis Weinstein Research Fund at the University of British Columbia. We would also like to thank the anonymous referee for support and useful comments.

REFERENCES

Abbott, B. P. et al. 2016a, Astrophys. J. Lett., 818, L22
—. 2016b, ArXiv e-prints
Abbott, B. P. et al. 2016, Phys. Rev. Lett., 116, 061102
Abbott, B. P. et al. 2016, Living Reviews in Relativity, 19
Abrial, P., Moudden, Y., Starck, J.-L., Fadili, J., Delabrouille, J., & Nguyen, M. K. 2008, Statistical Methodology, 5, 289
Ahn, C. P. et al. 2012, Astrophys. J. Suppl., 203, 21
—. 2014, Astrophys. J. Suppl., 211, 17
Bartos, I., Crotts, A. P. S., & Márka, S. 2015, Astrophys. J. Lett., 801, L1
Belczynski, K., Holz, D. E., Bulik, T., & O'Shaughnessy, R. 2016, ArXiv e-prints, 1602.04531
Berry, C. P. L. et al. 2015, Astrophys. J., 804, 114
Bilicki, M., Jarrett, T. H., Peacock, J. A., Cluver, M. E., & Steward, L. 2014, Astrophys. J. Suppl., 210, 9
Bobin, J., Starck, J.-L., Fadili, J. M., Moudden, Y., & Donoho, D. L. 2007, IEEE Transactions on Image Processing, 16, 2675
Caiazzo, I., Antolini, E., & Heyl, J. S. 2016, in prepartion
Cerioli, A., Lodato, G., & Price, D. J. 2016, Mon. Not. Roy. Ast. Soc., 457, 939
Colless, M. et al. 2001, Mon. Not. Roy. Ast. Soc., 328, 1039
—. 2003, ArXiv Astrophysics e-prints, astro-ph/0306581
Connaughton, V. et al. 2016, ArXiv e-prints, 1602.03920
Dominik, M. et al. 2015, Astrophys. J., 806, 263
D'Orazio, D. J., Levin, J., Murray, N. W., & Price, L. 2016, ArXiv e-prints, 1601.00017
Driver, S. P., Liske, J., Cross, N. J. G., De Propris, R., & Allen, P. D. 2005, Mon. Not. Roy. Ast. Soc., 360, 81
East, W. E., Paschalidis, V., Pretorius, F., & Shapiro, S. L. 2016, Phys. Rev. D, 93, 024011
Eldridge, J. J. & Stanway, E. R. 2016, ArXiv e-prints, 1602.03790
Fan, X., Messenger, C., & Heng, I. S. 2015, Gravitational Wave Astrophysics: Proceedings of the Third Session of the Sant Cugat Forum on Astrophysics, ed. F. C. Sopuerta (Cham: Springer International Publishing), 35–42
Fermi-LAT collaboration. 2016, ArXiv e-prints, 1602.04488
Fernández, R. & Metzger, B. D. 2015, ArXiv e-prints, 1512.05435
Gehrels, N., Cannizzo, J. K., Kanner, J., Kasliwal, M. M., Nissanke, S., & Singer, L. P. 2015, ArXiv e-prints, 1508.03608
Gerosa, D., Kesden, M., O'Shaughnessy, R., Klein, A., Berti, E., Sperhake, U., & Trifirò, D. 2015, Physical Review Letters, 115, 141102
Ghosh, S. & Nelemans, G. 2015, Gravitational Wave Astrophysics: Proceedings of the Third Session of the Sant Cugat Forum on Astrophysics, ed. F. C. Sopuerta (Cham: Springer International Publishing), 51–58
Górski, K. M., Hivon, E., Banday, A. J., Wandelt, B. D., Hansen, F. K., Reinecke, M., & Bartelmann, M. 2005, Astrophys. J., 622, 759
Hambly, N. C., Davenhall, A. C., Irwin, M. J., & MacGillivray, H. T. 2001a, Mon. Not. Roy. Ast. Soc., 326, 1315
Hambly, N. C., Irwin, M. J., & MacGillivray, H. T. 2001b, Mon. Not. Roy. Ast. Soc., 326, 1295
Hambly, N. C. et al. 2001c, Mon. Not. Roy. Ast. Soc., 326, 1279
Hanna, C., Mandel, I., & Vousden, W. 2014, The Astrophysical Journal, 784, 8
Heyl, J., Colless, M., Ellis, R. S., & Broadhurst, T. 1997, Mon. Not. Roy. Ast. Soc., 285, 613
Huchra, J. P. et al. 2012, Astrophys. J. Suppl., 199, 26
Jarrett, T. 2004, Publ. Ast. Soc. Aust., 21, 396
Jarrett, T.-H., Chester, T., Cutri, R., Schneider, S., Rosenberg, J., Huchra, J. P., & Mader, J. 2000a, Astron. J., 120, 298
Jarrett, T. H., Chester, T., Cutri, R., Schneider, S., Skrutskie, M., & Huchra, J. P. 2000b, Astron. J., 119, 2498
Jones, D. H. et al. 2004, Mon. Not. Roy. Ast. Soc., 355, 747

—. 2009, Mon. Not. Roy. Ast. Soc., 399, 683
Kasliwal, M. M. & Nissanke, S. 2014, Astrophys. J. Lett., 789, L5
Kawaguchi, K., Kyutoku, K., Shibata, M., & Tanaka, M. 2016, ArXiv e-prints, 1601.07711
Kyutoku, K., Ioka, K., Okawa, H., Shibata, M., & Taniguchi, K. 2015, Phys. Rev. D, 92, 044028
Leibler, C. N. & Berger, E. 2010, Astrophys. J., 725, 1202
Liske, J., Lemon, D. J., Driver, S. P., Cross, N. J. G., & Couch, W. J. 2003, Mon. Not. Roy. Ast. Soc., 344, 307
Margalit, B. & Piran, T. 2015, Mon. Not. Roy. Ast. Soc., 452, 3419
Mingarelli, C. M. F., Levin, J., & Lazio, T. J. W. 2015, Astrophys. J. Lett., 814, L20
Nissanke, S., Kasliwal, M., & Georgieva, A. 2013, Astrophys. J., 767, 124
Norberg, P. et al. 2002, Mon. Not. Roy. Ast. Soc., 336, 907
Nuttall, L. K. & Sutton, P. J. 2010, Phys. Rev. D, 82, 102002
Saunders, W. et al. 2000, Mon. Not. Roy. Ast. Soc., 317, 55
Siegel, D. M. & Ciolfi, R. 2015a, ArXiv e-prints, 1508.07911
—. 2015b, ArXiv e-prints, 1508.07939
Singer, L. P. & Price, L. R. 2016, Phys. Rev. D, 93, 024013
Singer, L. P. et al. 2014, Astrophys. J. Suppl., 211, 7
—. 2016a, ArXiv e-prints
—. 2016b, ArXiv e-prints
Skrutskie, M. F. et al. 2006, Astron. J., 131, 1163
Smartt, S. J. et al. 2016, ArXiv e-prints, 1602.04156
Soares-Santos, M. et al. 2016, ArXiv e-prints, 1602.04198
Staveley-Smith, L. et al. 1996, Publ. Ast. Soc. Aust., 13, 243
Vanderlinde, K. & Chime Collaboration. 2014, in Exascale Radio Astronomy, Vol. 2
Wright, E. L. et al. 2010, Astron. J., 140, 1868
Yang, H. & Zhang, F. 2016, Astrophys. J., 817, 183